A New Volume Integral Formulation for Broadband 3-D Circuit Extraction in Inhomogeneous Materials With and Without External Electromagnetic Fields

Saad Omar, *Student Member, IEEE*, and Dan Jiao, *Senior Member, IEEE*

***Abstract*—A new first-principles-based volume integral equation (VIE) formulation is developed for the broadband full-wave extraction of general 3-D circuits, containing arbitrarily shaped lossy conductors with inhomogeneous dielectrics. The proposed formulation accentuates all the advantages of the VIE formulation traditionally developed for solving wave-related problems, while allowing for the extraction of multiport circuit parameters such as impedance Z-, admittance Y-, and scattering S-parameters at ports located anywhere in the physical structure of a circuit. Its first-principles-based formulation without circuit-based simplifications and approximations can also be utilized to analyze the performance of a circuit in adverse ambient conditions, such as the exposure to strong external electromagnetic fields. In addition, the magneto-quasi-static and electro-magneto-quasi-static counterparts of the proposed full-wave formulation are also given for low-frequency applications. Numerical experiments have validated the accuracy and capability of the proposed new VIE formulation.**

***Index Terms*—Broadband analysis, circuit modeling, external electromagnetic fields, full-wave analysis, impedance extraction, *S*-parameter extraction, 3-D structures, volume integral equations (VIEs).**

I. Introduction

ELECTRONIC circuits operating in a densely integrated environment, military integrated circuits in the battlefield, microwave, and RF circuits in communication satellites can be exposed to strong external fields. Circuit modeling techniques ignoring such severe, yet practical ambient conditions can potentially lead toward catastrophic design failures. The circuits used for military applications require a high order of sensitivity and accuracy. These circuits cannot sustain those operating environments that were not catered during their design process. Although there have been many developments in circuit extraction techniques, little work has been reported in circuit parameter extraction with (explicitly defined) external electromagnetic fields taken into consideration. The underlying problem is both a circuit and a scattering problem, thus challenging to solve. The physical layout of the problem under analysis can be viewed as a "circuit" only to the internal circuit sources. However, the same physical layout behaves as a "scatterer" to external electromagnetic fields.

The problem of a circuit exposed to external electromagnetic fields is an open-region problem, which is different from traditional problems considered in circuit design. To model open-region problems, integral-equation (IE)-based solvers are more efficient than partial-differential-equation-based solvers since they avoid the use of any artificial absorbing boundary condition and they handle the open-region radiation condition analytically. There are two major classes of IE-based solvers: surface IE-based solvers and volume integral equation (VIE)-based ones. Compared to surface IE-based solvers [1]–[5] for broadband circuit modeling, VIE-based solvers have a greater capability in handling inhomogeneous dielectric and conductive materials, both of which are common in integrated circuits.

The VIE has been used to derive an equivalent circuit model from physical geometry in the partial-element equivalent-circuit (PEEC) method [6]–[9]. It has also been employed to perform a quasi-static analysis to extract frequency-dependent resistances and inductances of 3-D lossy conductor networks [10], [11]. The PEEC-based VIE formulation has also been combined with the equivalent charge method for impedance extraction in multiple dielectrics [12]. These circuit-orientated VIE methods for circuit modeling involve certain treatments and simplifications that are not used in a VIE-based solver developed for analyzing wave-related problems such as propagation, radiation, and scattering problems [13]. In addition, they have not taken external electromagnetic fields into consideration in circuit model generation.

The VIE solver for wave problems [13]–[18] entails no theoretical approximations or simplifications. It is theoretically valid in a full electromagnetic spectrum. It formulates a VIE for both fields inside nonperfect conductors and fields outside conductors in the inhomogeneous materials that are different from the background material. With a tetrahedron-element-based discretization, it offers great flexibility in modeling arbitrarily shaped conductors and dielectrics. With vector basis functions, it is capable of capturing both conduction and displacement currents flowing along an arbitrary direction inside conductor networks and dielectric materials. Despite the aforementioned advantages, the VIE solvers developed for wave problems have been found not amenable for solving circuit problems. This is because for solving wave-related problems, an incident field or a delta-gap voltage source [21] is generally used in the VIE

Manuscript received July 04, 2013; revised September 08, 2013; accepted September 30, 2013. Date of publication October 25, 2013; date of current version December 02, 2013. This work was supported by the National Science Foundation (NSF) under Grant 0747578, the Semiconductor Research Corporation (SRC) under a grant (Task 1292.073), and the Office of Naval Research (ONR) under Grant N00014-10-1-0482. This paper is an expanded paper from the IEEE MTT-S International Microwave Symposium, Seattle, WA, USA, June 2–7, 2013.

The authors are with the School of Electrical and Computer Engineering, Purdue University, West Lafayette, IN 47907 USA.

Color versions of one or more of the figures in this paper are available online at http://ieeexplore.ieee.org.

Digital Object Identifier 10.1109/TMTT.2013.2285355

solver as the excitation. Although the formulation is convenient for scattering and radiation analysis, it is difficult to be adopted for circuit parameter extraction at ports that can be located anywhere in the physical layout of a circuit. For port-parameter extraction, the delta-gap source model is generally used. This model requires two ports to be very close to each other, and also it introduces a piece of conductor to fill the gap between the two ports. Although there have been many enhancements to the delta-gap source model such as [22], [23], this source model cannot be adopted for circuit parameter extraction at ports located anywhere in the physical layout of a circuit.

The contribution of this work is the development of a new first-principles-based full-wave VIE formulation for the extraction of general 3-D circuits having arbitrarily shaped lossy conductors and inhomogeneous dielectrics exposed to external electromagnetic fields or without external fields. This formulation retains the first-principles-based accuracy and all the inherent flexibility of the VIE formulation developed for solving wave problems, while allowing for the extraction of multiport circuit parameters, such as impedance, admittance, and scattering parameters, at any port of interest, and from low to any electrodynamic frequency. Moreover, the first-principles accuracy of the proposed new formulation permits the analysis of circuit performance in a severe ambient environment, such as strong external fields, which has rarely been studied before. This formulation can also be straightforwardly modified to an electro-magneto-quasi-static (EMQS) or magneto-quasi-static (MQS) formulation for circuit parameter extraction at low frequencies. Numerical experiments have demonstrated its accuracy and added capability. We have presented the basic idea of this work in [19]. In this paper, we complete it from both theoretical and numerical perspectives.

The remainder of this paper is organized as follows. In Section II, we formulate the proposed new VIE that is applicable to circuit, scattering, and simultaneous circuit-scattering analysis. In Section III, the discretization of the proposed VIE formulation is given and the construction of the system matrix is detailed. In Section IV, we demonstrate the accuracy and capability of the proposed new VIE formulation through a suite of on-chip and package examples without external electromagnetic fields or exposed to external fields. The concluding remarks are included in Section V.

II. Proposed New VIE Formulation for Broadband Circuit Modeling in Inhomogeneous Materials With and Without External Fields

Consider a general 3-D circuit with a union of arbitrarily shaped conductors of finite conductivity σ_i, and hence, a complex permittivity $\bar{\epsilon}_i = (\epsilon_0 - j\sigma_i/\omega)$, and permeability μ_i. These conductors are embedded in inhomogeneous dielectrics that can be lossless, lossy, and dispersive. Both conductors and dielectrics are characterized by space-dependent complex permittivity $\bar{\epsilon}(\vec{r}) = (\epsilon_r(\vec{r})\epsilon_0 - j\sigma(\vec{r})/\omega)$ with ϵ_r being the dielectric constant. The background material is assumed to be free space having permittivity ϵ_0. It can also be another material. The circuit can be simultaneously exposed to internal circuit sources and external electromagnetic fields, such as an incident plane wave in a broad band of frequencies.

A. Full-Wave Formulation

When a circuit is exposed to an incident field $\vec{E}^i(\vec{r})$, based on the volume equivalence principle, the equivalent volume current $\vec{J} = j\omega(\bar{\epsilon} - \epsilon_0)\vec{E}$ radiating in the background material produces the scattered field. Thus, the total field $\vec{E}$ at any point $\vec{r}$ is equal to the sum of the incident field and the scattered field

$$\vec{E}(\vec{r}) + \nabla\phi^s(\vec{r}) + j\omega A^s(\vec{r}) = \vec{E}^i(\vec{r}) \tag{1}$$

which is expressed in the following form of the VIE [13]:

$$\frac{\vec{D}(\vec{r})}{\bar{\epsilon}(\vec{r})} - \mu\omega^2 \int_V \kappa(\vec{r'})\vec{D}(\vec{r'})g(\vec{r},\vec{r'})dv' - \nabla \int_V \nabla' \cdot \left(\frac{\kappa(\vec{r'})\vec{D}(\vec{r'})}{\epsilon_0}\right) g(\vec{r},\vec{r'})dv' = \vec{E}^i(\vec{r}) \tag{2}$$

where Green's function $g(\vec{r},\vec{r'}) = e^{-jk_0|\vec{r}-\vec{r'}|}/4\pi|\vec{r}-\vec{r'}|$, ω being the angular frequency, k_0 is the free-space wavenumber, κ is the contrast ratio defined as

$$\kappa(\vec{r}) = \frac{\bar{\epsilon}(\vec{r}) - \epsilon_0}{\bar{\epsilon}(\vec{r})} \tag{3}$$

and $\vec{D}(\vec{r})$ is

$$\vec{D}(\vec{r}) = \bar{\epsilon}(r)\vec{E} \tag{4}$$

which is related to the equivalent volume current by $\vec{J}(\vec{r}) = j\omega\kappa(\vec{r})\vec{D}(\vec{r})$. From the third term in (2), it can be seen that the scattering potential ϕ^s, at any point $\vec{r}$, is given by

$$\phi^s(\vec{r}) = -\int_V \nabla' \cdot \left(\frac{\kappa(\vec{r'})\vec{D}(\vec{r'})}{\epsilon_0}\right) g(\vec{r},\vec{r'})dv' \tag{5}$$

which can further be written as

$$\phi^s(\vec{r}) = \int_V \frac{\rho_v(\vec{r'})}{\epsilon_0} g(\vec{r},\vec{r'})dv' + \int_S \frac{\rho_s(\vec{r'})}{\epsilon_0} g(\vec{r},\vec{r'})ds' \tag{6}$$

where ρ_v is the density of equivalent volume charges (volume polarization charges), and ρ_s is the density of the equivalent surface charges (surface polarization charges) at the material discontinuity where $\kappa(\vec{r})$ is discontinuous. ρ_v and ρ_s have a relationship with $\vec{D}$, which can be derived from (5) as follows:

$$\begin{aligned} \rho_v(\vec{r'}) &= -\kappa(\vec{r'})\nabla' \cdot \vec{D}(\vec{r'}) \\ \rho_s(\vec{r'}) &= (\kappa^+(\vec{r'}) - \kappa^-(\vec{r'}))\vec{D}(\vec{r'}) \cdot \hat{n} \end{aligned} \tag{7}$$

in which superscripts $-$ and $+$ are the indices of the two materials at a material discontinuity, and $\hat{n}$ denotes a unit vector normal to the material interface and pointing from material $+$ to material $-$. It is worth mentioning that although the divergence of $\vec{D}$ is zero in a source-free region, this condition is not explicitly satisfied in the VIE formulation since this condition has been satisfied implicitly by the Ampere's law used to build the VIE formulation. The vector basis functions employed to expand $\vec{D}$ such as the Schaubert–Wilton–Glisson (SWG) bases also have a nonzero divergence.

In analyzing wave-related problems, the incident field $\vec{E}^i(\vec{r})$ is chosen either as an incident plane wave or a delta-gap voltage source. Neither of them is suitable for multiport circuit parameter extraction where ports can be physically located anywhere

in the layout of an integrated circuit. In contrast, an electric potential ϕ-based excitation facilitates the extraction of multiport circuit parameters. We can attach each port in turn to an electric potential, while grounding all the other ports, to obtain the current at each port, from which the circuit parameters such as admittance ($\mathbf{Y}$), scattering ($\mathbf{S}$), and impedance ($\mathbf{Z}$) parameters can be obtained. Surface IE-based methods in [1] and [2] are capable of accommodating a ϕ-based excitation by introducing potential and charge as additional unknowns. However, as can be seen from (2), the only unknowns in the traditional VIE formulation for solving Maxwell's equations is $\vec{D}$, and the potential and charge unknowns are not necessary. In order to incorporate the electric-potential-based excitation while preserving the first-principles-based nature of the original wave-based VIE formulation shown in (2), we propose a new VIE formulation as follows. The essential idea of the proposed formulation can also be applied to the surface IEs to incorporate an electric potential-based excitation.

When the circuit is attached to a potential source, the total potential ϕ is known at the contact surface where the source is attached. Instead of solving (1), we solve

$$\vec{E}(\vec{r}) = -\nabla\phi(\vec{r}) - j\omega\vec{A}(\vec{r}) \tag{8}$$

subject to

$$\phi(\vec{r}_c) = \Psi_c \tag{9}$$

where $\vec{r}_c$ denotes a point on the contact surface, where potential Ψ_c is applied. Equation (8) can further be written as

$$\frac{\vec{D}(\vec{r})}{\bar{\epsilon}(\vec{r})} - \mu\omega^2 \int_V \kappa(\vec{r'})\vec{D}(\vec{r'})g(\vec{r},\vec{r'})dv' + \nabla\phi(\vec{r}) = 0 \tag{10}$$

where the potential ϕ is generated by equivalent volume charges and equivalent surface charges at the material discontinuity, which is the same as that shown in (6). However, one has to realize one key difference in order to develop a correct first-principles-based VIE formulation for modeling a potential-based excitation. To explain, in the case of the incident field $\vec{E}^i(\vec{r})$-based excitation, the relationship between charge densities (ρ_v and ρ_s) and $\vec{D}$ is known as shown in (7). Therefore, we only need to solve for $\vec{D}$ to obtain the circuit response to the incident field. In other words, the only unknown contained in (1), and hence (2), is $\vec{D}$. In contrast, in the case of the potential-based excitation, since the contact surface is now attached to potential Ψ_c, the equivalent surface charge density ρ_s on the contact surface, denoted by ρ_{cs}, is unknown, whereas the relationship between $\vec{D}$ and other charge densities, i.e., ρ_v and ρ_s not belonging to the contact surfaces, remains intact as that shown in (7). Therefore, for circuits attached to a potential-based source, we solve for $(\vec{D}, \rho_{cs})$. To be more specific, the ϕ in (10) can be written as

$$\begin{aligned}\phi(\vec{r}) = &-\int_V \kappa(\vec{r'})\nabla'\cdot\left(\frac{\vec{D}(\vec{r'})}{\epsilon_0}\right)g(\vec{r},\vec{r'})dv' \\ &+\int_{S\notin S_c}\frac{(\kappa^+(\vec{r'})-\kappa^-(\vec{r'}))\vec{D}\cdot\hat{n}}{\epsilon_0}g(\vec{r},\vec{r'})ds' \\ &+\int_{S_c}\frac{\rho_{cs}(\vec{r'})}{\epsilon_0}g(\vec{r},\vec{r'})ds'\end{aligned} \tag{11}$$

where S denotes the union of all the interfaces at the material discontinuity, while S_c represents the contact surface. As a result, the unknowns contained in (8), and hence (10), are both $\vec{D}$ and ρ_{cs}. Although ρ_{cs} are additional unknowns, $\phi(\vec{r}_c) = \Psi_c$ in (9) provides the same number of additional equations to complete the numerical system. To summarize, when a circuit is attached to a potential source, we solve the following two equations simultaneously:

$$\begin{aligned}&\frac{\vec{D}(\vec{r})}{\bar{\epsilon}(\vec{r})} - \mu\omega^2\int_V \kappa(\vec{r'})\vec{D}(\vec{r'})g(\vec{r},\vec{r'})dv' \\ &\quad-\nabla\int_V \kappa(\vec{r'})\nabla'\cdot\left(\frac{\vec{D}(\vec{r'})}{\epsilon_0}\right)g(\vec{r},\vec{r'})dv' \\ &\quad+\nabla\int_{S\notin S_c}\frac{(\kappa^+(\vec{r'})-\kappa^-(\vec{r'}))\vec{D}\cdot\hat{n}}{\epsilon_0}g(\vec{r},\vec{r'})ds' \\ &\quad+\nabla\int_{S_c}\frac{\rho_{cs}(\vec{r'})}{\epsilon_0}g(\vec{r},\vec{r'})ds' \\ &= 0\end{aligned} \tag{12}$$

$$\begin{aligned}&-\int_V \kappa(\vec{r'})\nabla'\cdot\left(\frac{\vec{D}(\vec{r'})}{\epsilon_0}\right)g(\vec{r}_c,\vec{r'})dv' \\ &\quad+\int_{S\notin S_c}\frac{(\kappa^+(\vec{r'})-\kappa^-(\vec{r'}))\vec{D}\cdot\hat{n}}{\epsilon_0}g(\vec{r}_c,\vec{r'})ds' \\ &\quad+\int_{S_c}\frac{\rho_{cs}(\vec{r'})}{\epsilon_0}g(\vec{r}_c,\vec{r'})ds' \\ &= \Psi_c.\end{aligned} \tag{13}$$

As can be seen from the above derivation, in the proposed VIE formulation, we do not introduce potential ϕ, volume charge density ρ_v, noncontact surface charge density as additional unknowns for circuit parameter extraction. Instead, we only introduce ρ_{cs} as an extra unknown, which is necessary to satisfy the known potential condition at the contact surface. As a result, all the first-principles features of the original wave-based VIE are preserved for the following reasons. Firstly, the formulation is truly full wave, which is valid in a full electromagnetic spectrum from low to electrodynamic frequencies. Secondly, the formulation is equally applicable to problems with a uniform material and problems with complicated inhomogeneous materials without any need for change. Thirdly, not only the current inside the nonperfect conductors is modeled, but also the displacement current outside conductors is captured in the inhomogeneous materials different from the background material. Lastly, the formulation can be used to capture currents flowing along an arbitrary direction both inside conductor networks and outside conductors in the inhomogeneous materials. Moreover, the proposed new VIE formulation facilitates the circuit network parameter extraction at ports located anywhere in the physical layout of the circuit. This is because the potential source can be attached to any physical point without any difficulty in numerical simulation. Owing to its first-principles-based accuracy without circuit-based simplifications and approximations, in conjunction with (2), the proposed formulation also permits the analysis of a circuit exposed to both internal circuit sources and external electromagnetic fields, the problem that is both a scattering and a circuit problem.

B. MQS and EMQS Formulation

The full-wave VIE formulation developed in Section II-A can also be modified to perform analyses in MQS and EMQS settings for applications with relatively small electric sizes. When the entire structure being simulated is electrically small, the static and/or quasi-static physics can be utilized to simplify the analysis and generate a better-conditioned numerical system. In an EMQS analysis, we reduce the Green's function in the proposed full-wave formulation to its static form. In a MQS analysis, since the displacement current is ignored and $\nabla \cdot \vec{J} = 0$, all the charges become zero. As a result, ϕ^s in (6) is zero and there is no $\phi - \rho$ relationship shown in (11) anymore. In this case, for the incident-field-based excitation, we set ϕ^s to be zero in (1), and hence (2), to perform a MQS analysis. For the potential-based excitation, we solve the following equations:

$$\frac{\vec{D}(\vec{r})}{\bar{\epsilon}(\vec{r})} - \mu\omega^2 \int_V \kappa(\vec{r'})\vec{D}(\vec{r'})g_{qs}(\vec{r},\vec{r'})dv' + \nabla\phi(\vec{r}) = 0 \quad (14)$$

$$\phi(\vec{r}_c) = \Psi_c \quad (15)$$

$$\nabla \cdot \vec{D}(\vec{r}) = 0 \quad \vec{r} \in V \quad (16)$$

$$\vec{D}(\vec{r}_{\rm nc}) \cdot \hat{n} = 0 \quad (17)$$

where g_{qs} denotes the static counterpart of the Green's function g, $\vec{r}_{\rm nc}$ denotes a point on the noncontact surface, the third equation ensures the volume polarization charge density ρ_v to be zero, while the fourth equation sets the surface polarization charges on the noncontact surfaces to be zero. Since now $j\omega\vec{D}$ becomes just conduction current $\sigma\vec{E}$ as the displacement current is ignored, the computational domain that includes both dielectric and conductor regions is also reduced to conductor regions only in a MQS analysis. Notice that in the above equation, $\vec{D}$ and ϕ are solved instead of $\vec{D}$ and ρ solved in the full-wave case. This is because the charges are zero in the MQS analysis, the relationship between ϕ and charges does not exist. Hence, in the VIE, ϕ also becomes unknowns to be solved, except for the ϕ on the contact surfaces (points), but the condition of zero volume and surface charges yields the same number of equations as the number of ϕ unknowns, thus completing the numerical system. In addition to EMQS and MQS analyses, the proposed full-wave formulations can also be straightforwardly reduced to static formulations.

C. Circuit Parameter Extraction

For multiport circuit parameter extraction where ports can be located anywhere in a circuit, we attach each port in turn to the given potential Ψ_c by setting $\phi = \Psi_c \neq 0$ at the port, while attaching the rest of the ports to $\phi = \Psi_c = 0$. Owing to the flexibility of the proposed formulation, $\phi = \Psi_c$ can be set at a location as small as a point. Therefore, one can either let $\phi = \Psi_c$ be satisfied at one point $\vec{r}$, a few points, or the whole area of the port depending on the port area that is actually contacted by the potential source. With the potential-based excitation, $\vec{D}$ is solved from the proposed VIE formulations. The current at any port of the circuit can then be computed as follows:

$$I = j\omega \int_{\rm Xsec} \vec{D} \cdot \hat{n} ds \quad (18)$$

where Xsec represents the cross-sectional area of the conductor at the port, and $\hat{n}$ is a unit vector normal to Xsec. Xsec can be as small as a single triangular patch. From the known potential and the current computed at each port, we can obtain any kind of network parameters such as admittance ($\mathbf{Y}$)-, impedance ($\mathbf{Z}$)-, and scattering ($\mathbf{S}$)-parameters.

III. System Matrix Construction

We discretize the computational domain into tetrahedral elements. In each tetrahedral element, the unknown electric displacement $\vec{D}(\vec{r})$ is expanded into SWG basis functions $\vec{f}_n(\vec{r})$[13], the coefficient of which is denoted by D_n. Each of the SWG basis function is defined for a face of a tetrahedron. The basis function associated with the nth face common to tetrahedra T^+ and T^- is defined as follows:

$$F_n(r) = \begin{cases} \dfrac{a_n}{3V^+}\rho_n^+, & \text{r} \in T^+ \\ \dfrac{a_n}{3V^-}\rho_n^-, & \text{r} \in T^- \\ 0, & \text{otherwise.} \end{cases}$$

A. Full-Wave Formulation

1) External Field Excitation: For the external-field-based excitation, we solve (2). By expanding the unknown $\vec{D}$ in each element by the SWG basis, and also testing (2) using the same basis, we obtain

$$\begin{aligned} &\int_{V_m} \vec{f}_m(\vec{r}) \cdot \vec{E}^i(\vec{r}) dv \\ &= \sum_{n=1}^{N} D_n \Bigg[\int_{V_m} \vec{f}_m(\vec{r}) \cdot \frac{\vec{f}_n(\vec{r})}{\bar{\epsilon}(\vec{r})} dv \\ &\quad - \mu\omega^2 \int_{V_m}\int_{V_n} \kappa_n(\vec{r'})\vec{f}_m(\vec{r}) \cdot \vec{f}_n(\vec{r'}) g(\vec{r},\vec{r'}) dv' dv \\ &\quad - \frac{1}{\epsilon_0}\left(\int_{S_m}\int_{V_n} \kappa_n(\vec{r'})(\vec{f}_m(\vec{r}) \cdot \hat{n}_m)(\nabla' \cdot \vec{f}_n(\vec{r'})) \right) \\ &\quad \cdot g(\vec{r},\vec{r'}) dv' ds \\ &\quad - \int_{S_m}\int_{S_n} (\kappa_n^+(\vec{r'}) - \kappa_n^-(\vec{r'}))(\vec{f}_m(\vec{r}) \cdot \hat{n}_m) \\ &\quad \cdot (\vec{f}_n(\vec{r'}) \cdot \hat{n}_n) g(\vec{r},\vec{r'}) ds' ds \\ &\quad + \int_{V_m}\int_{V_n} \kappa_n(\vec{r'})(\nabla \cdot \vec{f}_m(\vec{r}))(\nabla' \cdot \vec{f}_n(\vec{r'})) \\ &\quad \cdot g(\vec{r},\vec{r'}) dv' dv \\ &\quad - \int_{V_m}\int_{S_n} (\kappa_n^+(\vec{r'}) - \kappa_n^-(\vec{r'}))(\nabla \cdot \vec{f}_m(\vec{r})) \\ &\quad \cdot (\vec{f}_n(\vec{r'}) \cdot \hat{n}_n) g(\vec{r},\vec{r'}) ds' dv \Bigg). \end{aligned} \quad (19)$$

Rewriting the above in a matrix equation format, we obtain

$$\mathbf{Z}D = E \quad (20)$$

where the mth entry of vector E is

$$E_m = \int_{V_m} \vec{f}_m(\vec{r}) \cdot \vec{E}^i(\vec{r}) dv \quad (21)$$

and the $\mathbf{Z}$-matrix element at the mth row and the nth column, $\mathbf{Z}_{mn}$, is the term shown in the square bracket in (19).

It is worth noting that the parenthesized third term in $\mathbf{Z}_{mn}$, which itself has four components, denotes the potential observed at either an outermost boundary surface triangular patch (obtained by integrating over S_m) or an internal patch (obtained by integrating over V_m) due to contributions from both volume polarization charges ρ_v and surface polarization charges ρ_s. Another important fact is that the material discontinuity also occurs at the outermost boundary of the structure.

2) Potential-Based Excitation: When the circuit is attached to an electric potential, the new unknown ρ_{cs} is expanded by the pulse basis functions, i.e., being a constant on each triangular patch. The Galerkin method is applied to test (12), while the centroid collocation method is applied to test (13). The resulting system of linear equations can be written as

$$\begin{aligned} \mathbf{Z^r}[D_n] + \mathbf{Z^t}[\rho_{cs}] &= K_1 \\ \mathbf{P_0^p}[D_n] + \mathbf{P_0^{cs}}[\rho_{cs}] &= K_2 \end{aligned} \tag{22}$$

where matrices $\mathbf{Z^r}$ and $\mathbf{Z^t}$ can be viewed as the segregated versions of $\mathbf{Z}$ in (20). The contributions from the charges on the contact surface, ρ_{cs}, appear as entries of $\mathbf{Z^t}$, while all remaining contributions are carried by $\mathbf{Z^r}$. Mathematically,

$$\begin{aligned} &\mathbf{Z^r}_{mn} \\ &= \int_{V_m} \vec{f}_m(\vec{r}) \cdot \frac{\vec{f}_n(\vec{r})}{\bar{\epsilon}(\vec{r})} dv \\ &\quad - \mu\omega^2 \int_{V_m}\int_{V_n} \kappa_n(\vec{r'}) \vec{f}_m(\vec{r}) \cdot \vec{f}_n(\vec{r'}) g(\vec{r},\vec{r'}) dv' dv \\ &\quad - \frac{1}{\epsilon_0}\left(\int_{S_m \notin S_c}\int_{V_n} \kappa_n(\vec{r'}) (\vec{f}_m(\vec{r}) \cdot \hat{n}_m)(\nabla' \cdot \vec{f}_n(\vec{r'})) \right) \\ &\quad \cdot g(\vec{r},\vec{r'}) dv' ds \\ &\quad - \int_{S_m \notin S_c}\int_{S_n \notin S_c} (\kappa_n^+(\vec{r'}) - \kappa_n^-(\vec{r'}))(\vec{f}_m(\vec{r}) \cdot \hat{n}_m) \\ &\quad \cdot (\vec{f}_n(\vec{r'}) \cdot \hat{n}_n) g(\vec{r},\vec{r'}) ds' ds \\ &\quad + \int_{V_m}\int_{V_n} \kappa_n(\vec{r'}) (\nabla \cdot \vec{f}_m(\vec{r}))(\nabla' \cdot \vec{f}_n(\vec{r'})) g(\vec{r},\vec{r'}) dv' dv \\ &\quad - \int_{V_m}\int_{S_n \notin S_c} (\kappa_n^+(\vec{r'}) - \kappa_n^-(\vec{r'}))(\nabla \cdot \vec{f}_m(\vec{r})) \\ &\quad \cdot (\vec{f}_n(\vec{r'}) \cdot \hat{n}_n) g(\vec{r},\vec{r'}) ds' dv \Big) \end{aligned} \tag{23}$$

and

$$\begin{aligned} \mathbf{Z^t}_{mn} = \frac{1}{\epsilon_0}\Bigg(&\int_{S_m \notin S_c}\int_{S_n \in S_c} (\vec{f}_m(\vec{r}) \cdot \hat{n}_m) g(\vec{r},\vec{r'}) ds' ds \\ &+ \int_{V_m}\int_{S_n \in S_c} (\nabla \cdot \vec{f}_m(\vec{r})) g(\vec{r},\vec{r'}) ds' dv \Bigg). \end{aligned} \tag{24}$$

The contribution from all contact-surface patches is contained in the right-hand-side vector K_1 since the potential on the contact surface is known according to (9). Thus, we have

$$K_{1m} = -\int_{S_m \in S_c} (\vec{f}_m(\vec{r}) \cdot \hat{n}_m) \Psi_c ds. \tag{25}$$

The second row of (22) is nothing but the discretized equivalent of (9) with ϕ computed from (11). Its right-hand side is simply the potential on the contact-surface patches. Thus, K_2's entries are

$$K_{2m} = \Psi_c, m \in S_c. \tag{26}$$

The potential generated by the charges on the contact surface is shown by the third term in (11), from which $\mathbf{P_0^{cs}}$ in (22) can be obtained as

$$\mathbf{P_0^{cs}}_{mn} = \frac{1}{\epsilon_0}\Big(\int_{S_n \in S_c} g(\vec{r}_m, \vec{r'}) ds' \Big), \qquad \vec{r}_m \in S_c. \tag{27}$$

The potential contributed by all other charges is given by the first and second term in (11), from which we obtain

$$\begin{aligned} &\mathbf{P_0^P}_{mn} \\ &= \frac{1}{\epsilon_0}\Bigg(- \int_{V_n} \kappa(\vec{r'})(\nabla' \cdot \vec{f}_n(\vec{r'})) g(\vec{r}_m,\vec{r'}) dv' \\ &\qquad + \int_{S_n \notin S_c} (\kappa^+(\vec{r'}) - \kappa^-(\vec{r'})) \vec{f}_n(\vec{r'}) \cdot \hat{n} g(\vec{r}_m,\vec{r'}) ds' \Bigg), \\ &\quad \vec{r}_m \in S_c. \end{aligned} \tag{28}$$

The numerical system (22) can be used for full-wave circuit parameter extraction with a circuit source only, while the inclusion of (20) permits the full-wave analysis of a circuit exposed to external fields, interferences, radiations, etc. It is worth mentioning that for the latter problem, we cannot simply set the K_1 in the right-hand side of (22) to be the incident field for entries not belonging to the contact surface, while letting K_1 be (25) for contact-surface entries. This is because for the incident-field-based excitation, the surface charge density ρ_s at any material discontinuity is related to $\vec{D}$, as shown in (7). However, the same relationship does not hold true for the potential-based excitation at the contact surface. Therefore, instead of (6), (11) is used in (10) for solving the VIE for the potential-based excitation. In other words, the VIE equations to be solved are different for the two different excitations. Hence, we need to superpose the solutions obtained from (20) and (22) to analyze a circuit exposed to both internal circuit sources and external electromagnetic fields instead of keeping the left-hand-side matrix of (22) the same while using both excitations in the right-hand side.

B. Quasi-Static Analysis

For the VIE (14)–(17) derived for an MQS analysis, we solve for $(\vec{D}, \phi)$. Since the ϕ on the contact surface is known, we only need to solve for $(\vec{D}, \phi_v, \phi_{\rm ncs})$, where ϕ_v and $\phi_{\rm ncs}$ are the potentials on the centroid of each tetrahedral element, and at the center of each noncontact surface patch, respectively. The numerical system for (14)–(17) is again obtained by expanding $\vec{D}$ in each tetrahedral element by using SWG vector bases and then using Galerkin testing. ϕ_v and $\phi_{\rm ncs}$ are expanded by pulse basis functions, and the centroid collocation method is used to test (16), whereas (17) is applied at the center of each noncontact surface patch. Therefore, we obtain the following numerical system:

$$\begin{aligned} \mathbf{Z^{sr}}[D_n] + \mathbf{V^{t1}}[\phi_v] + \mathbf{V^{t2}}[\phi_{\rm ncs}] &= K_1 \\ \mathbf{\Sigma}[D_n] &= 0 \\ \mathbf{M}[D_n] &= 0 \end{aligned} \tag{29}$$

TABLE I
EXTRACTED IMPEDANCE PARAMETERS AT FULL-WAVE FREQUENCY POINTS

Frequency (GHz)	Data Type	Resistance (Ω)	Inductance (nH)
0.1	Proposed	0.038	1.45
	Reference	0.036	1.45
1.0	Proposed	0.216	1.45
	Reference	0.202	1.45

where

$$\mathbf{Z^{sr}}_{mn} = \int_{V_m} \frac{\vec{f}_m(\vec{r})}{\bar{\epsilon}(\vec{r})} \cdot \vec{f}_n(\vec{r}) dv - \mu\omega^2 \int_{V_m}\int_{V_n} \kappa(\vec{r'}) \vec{f}_m(\vec{r}) \cdot \vec{f}_n(\vec{r'}) g_{qs}(\vec{r}, \vec{r'}) dv' dv \quad (30)$$

$$\mathbf{V}^{t1}_{mn} = -\int_{V_m} (\nabla \cdot \vec{f}_m(\vec{r})) dv$$

$$\mathbf{V}^{t2}_{mn} = \int_{S_m} (\vec{f}_m(\vec{r}) \cdot \hat{n}_m) ds \quad (31)$$

and K_1 is the same as that shown in (25). The $\mathbf{\Sigma}$ matrix is a sparse matrix of dimension $N_V \times N$, where N_V and N are the number of tetrahedrons, and the total number of SWG bases, respectively. $\mathbf{\Sigma}_{mn}$ is nonzero only for those four bases that constitute the mth tetrahedron and given by

$$\mathbf{\Sigma}_{mn} = \int_{S_m} \vec{f}_m(\vec{r'}) \cdot \hat{n} ds'. \quad (32)$$

The $\mathbf{M}$ matrix is also a sparse matrix. Its dimension is $N_{\rm ncs} \times N$, where $N_{\rm ncs}$ is the number of noncontact surface patches. The $\mathbf{M}_{mn}$ is 1 only when the patch corresponding to the nth basis is a noncontact surface patch, i.e.,

$$\mathbf{M}_{mn} = \delta_{mn} \quad S_n \in S_{\rm nc} \quad (33)$$

in which $S_{\rm nc}$ denotes a noncontact surface.

IV. NUMERICAL RESULTS

In order to validate the proposed VIE formulations, we extract the impedance $\mathbf{Z}$-parameters of a straight conductor wire and those of a 1×5 on-chip bus structure. We also extract the $\mathbf{S}$-parameters of a package interconnect provided by a semiconductor company with and without inhomogeneous materials in a broad band of frequencies. In addition, we simulate circuits exposed to both external fields and internal circuit sources in order to demonstrate the capability of the proposed VIE solver in analyzing such problems. An irregularly shaped spiral inductor is also simulated to show the flexibility of the proposed VIE formulation in geometrical modeling.

A. Impedance Extraction of a Straight Conductor Wire

A conductor wire of dimension 1 mm × 1 mm × 4 mm is simulated in free space from 1 Hz to 1 GHz. The conductivity of the wire is 5.8×10^7 S/m. In order to capture the skin effect, the structure is discretized into 1200 tetrahedrons. We attach the near end of the wire to $\phi = 1$, and the far end to $\phi = 0$. In other

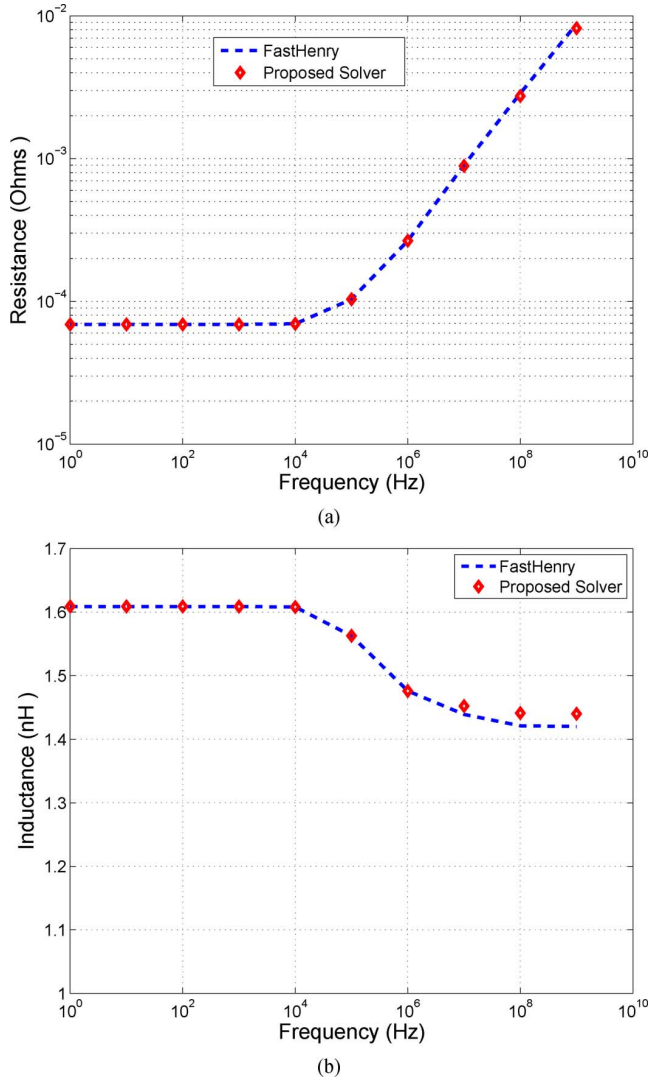

Fig. 1. Comparison of the impedance parameter of a straight wire conductor extracted from the proposed VIE solver and that from FastHenry. (a) Resistance (Ω). (b) Inductance (nH).

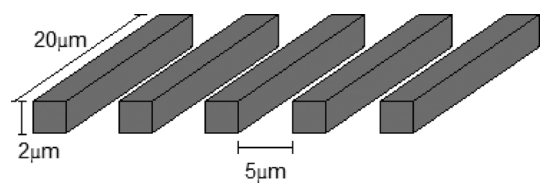

Fig. 2. Geometrical details of a 1 × 5 bus structure.

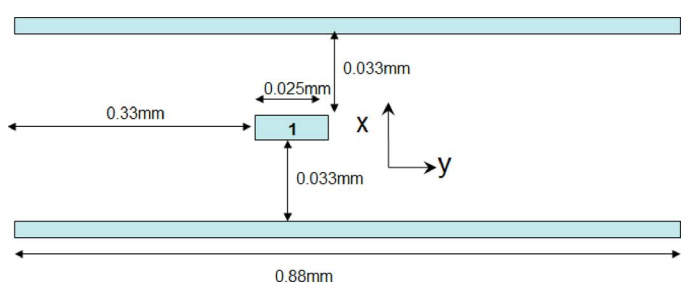

Fig. 3. Cross-sectional view of a 3-D package interconnect.

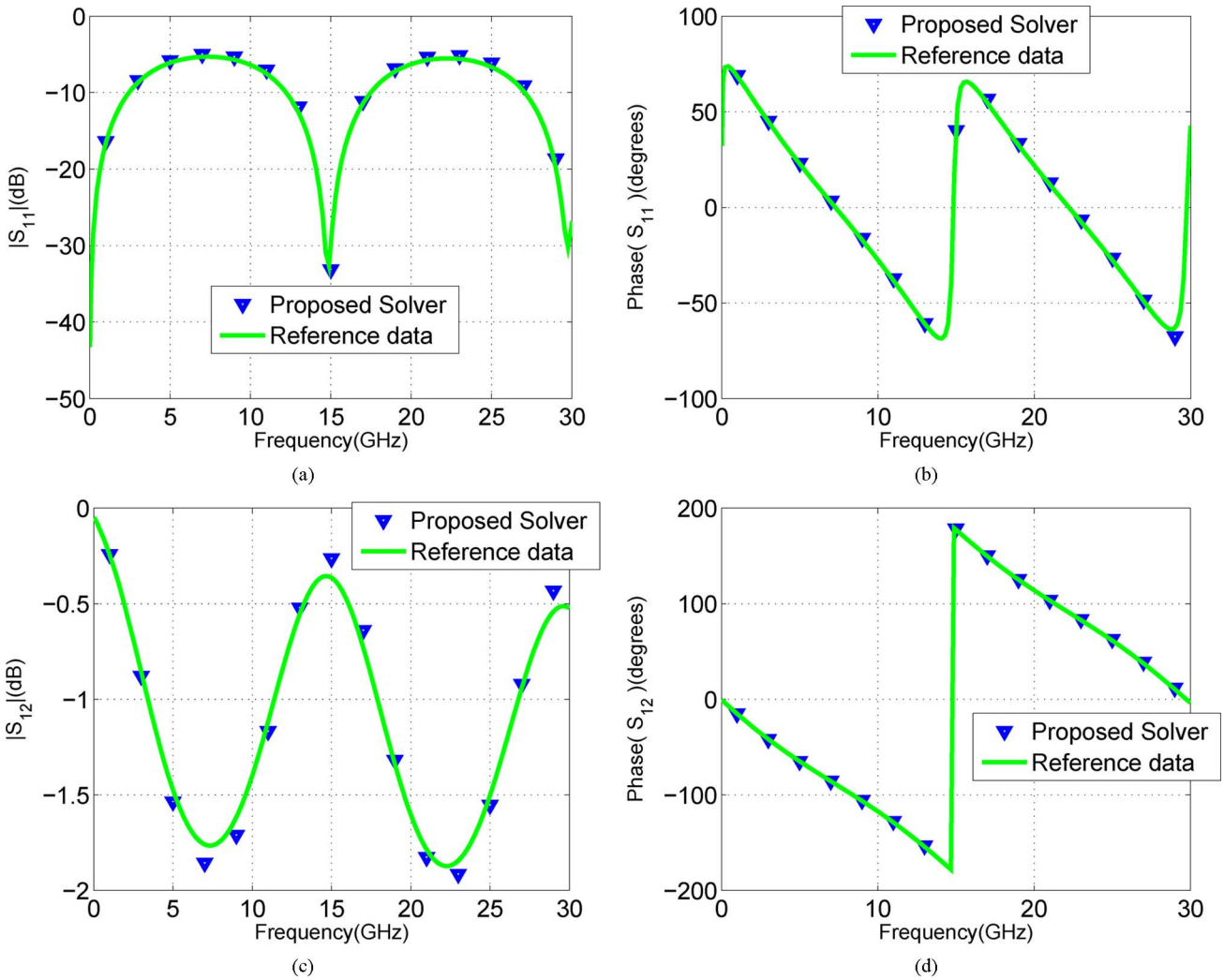

Fig. 4. S-parameters of a 3-D package interconnect with a uniform material simulated by the proposed full-wave VIE solver in comparison with reference data. (a) $|S_{11}|$ (dB). (b) S_{11} phase (degrees). (c) $|S_{12}|$ (dB). (d) S_{12} phase (degrees).

words, we let (9), and hence (13), be satisfied at the points located at the near end of the wire with $\Psi_c = 1$, and let (13) satisfied at the far-end points with $\Psi_c = 0$. After the current is solved from the proposed VIE formulation, the input impedance of the wire can be obtained by dividing the potential difference between the two wire ends by the current computed at the near end. The resistance and inductance can then be readily identified from the input impedance. The proposed VIE formulation in its MQS form is employed to carry out the simulation. The results are compared with the reference data generated by the MQS-based FastHenry [10] in Fig. 1 from 1 Hz to 1 GHz. Excellent agreement in impedance parameter can be observed, validating the proposed MQS-based VIE formulation.

The proposed full-wave VIE formulation is also used to simulate this example. It shows that at the last two frequency points (0.1 and 1 GHz), full-wave effects are actually pronounced, which cannot be captured by an MQS analysis. Hence, we compare the results generated from the proposed full-wave formulation with those obtained from a full-wave solver in [4]. As shown in Table I, the inductance value is the same, while there is a small difference in resistance, which can be attributed to

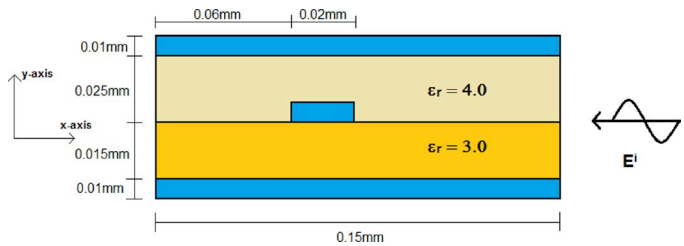

Fig. 5. Cross-sectional view of a multiple-dielectric package interconnect.

the volume-based discretization used in the proposed solver in contrast to the discretization used in the surface IE solver [4]. A comparison between the full-wave results shown in Table I and the MQS results depicted in Fig. 1 also reveals the inaccuracy of the MQS approximations at 0.1 and 1 GHz.

B. Impedance Extraction of a 1 × 5 On-Chip Bus

The second example is a 1×5 bus structure having typical on-chip dimensions in a single material (air). As illustrated in Fig. 2, each bus has a dimension of $2\ \mu\text{m} \times 2\ \mu\text{m} \times 20\ \mu\text{m}$, while

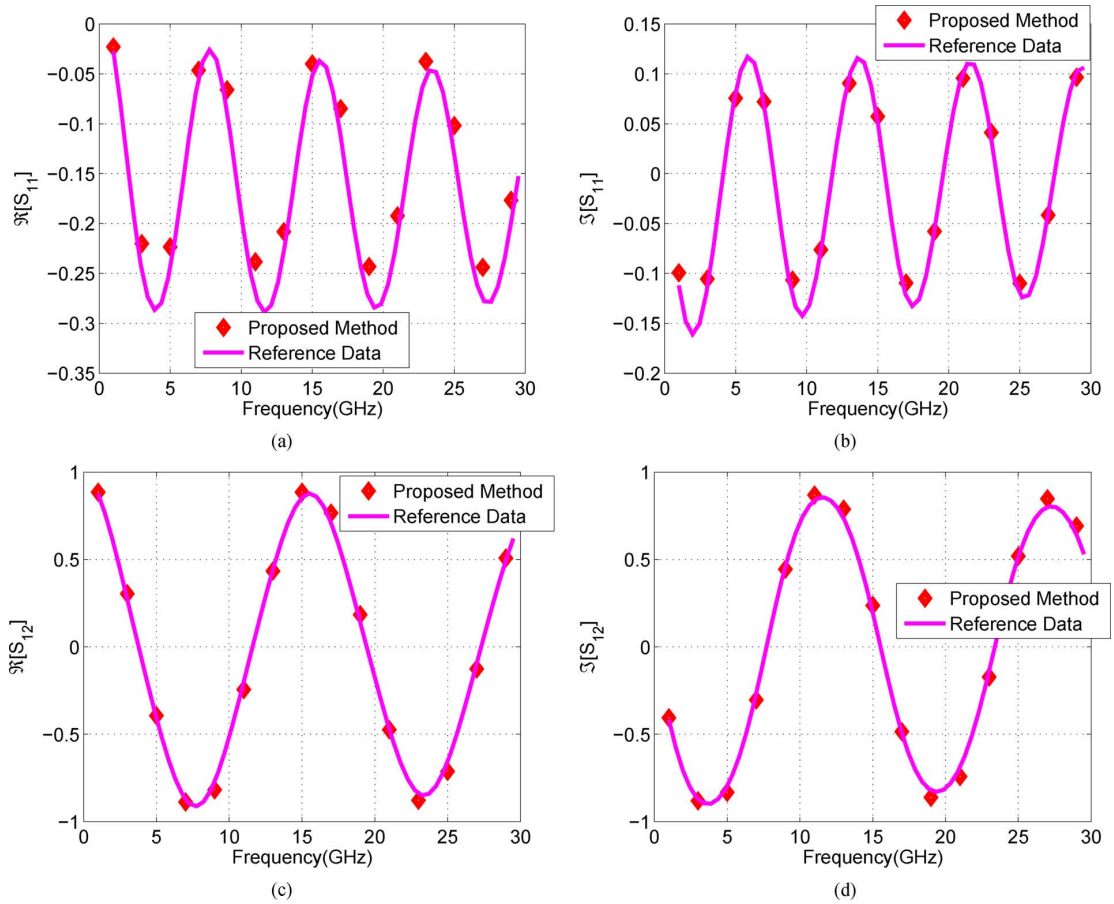

Fig. 6. S-parameters of a 3-D package interconnect with nonuniform materials simulated by the proposed full-wave VIE solver in comparison with reference data. (a) $\mathrm{Re}[S_{11}]$. (b) $\mathrm{Im}[S_{11}]$. (c) $\mathrm{Re}[S_{12}]$. (d) $\mathrm{Im}[S_{12}]$.

the spacing between two adjacent buses is 5 μm. The metal conductivity is again 5.8×10^7 S/m, and the frequency for extraction is 10 GHz. The discretization results in 6000 tetrahedrons. The impedance parameter matrix extracted from the proposed full-wave VIE formulation is given in the matrix shown at the bottom of this page. All impedances are in 10^{-2} Ω. The error of the above impedance matrix is shown to be 0.29%, computed from $\|\mathbf{Z}-\mathbf{Z}_{FH}\|_F/\|\mathbf{Z}_{FH}\|_F$, where $\mathbf{Z}_{FH}$ is obtained from FastHenry [10] with 12 000 filaments, $\mathbf{Z}$ is from the proposed full-wave VIE solver, and Frobenius norm is used. Since the full-wave effect is not dominant in this on-chip example due to its small electric size even at 10 GHz, we found that both MQS and full-wave solvers can produce accurate results for this example.

C. S-Parameter Extraction of a Package Interconnect

A 3-D package interconnect provided by IBM, the cross section of which is shown in Fig. 3, is extracted in a broad band of frequencies from 1 to 30 GHz. The interconnect has one metal plane on the top and one at the bottom, each of which is of width 0.88 mm. A center strip is of width 0.025 mm and its distance to the left boundary is 0.33 mm. The length of the structure is 1 cm. The background material is air. The conductivity of the metal is 5.8×10^7 S/m.

In Fig. 4, we plot the S-parameters extracted from the proposed full-wave VIE solver in comparison with the reference data provided by IBM in the entire simulated frequency band. Excellent agreement is observed in both magnitude and phase for all $\mathbf{S}$-parameters.

D. S-Parameter Extraction of a Package Interconnect With Multiple Dielectrics

A 3-D package interconnect with multiple dielectrics, whose detailed geometrical and material data are shown in Fig. 5, is extracted in a broad band of frequencies from 1 to 30 GHz. The

$$\begin{bmatrix} 10.128+71.349i & 0.105+26.699i & -0.052+16.037i & -0.034+11.322i & -0.019+8.706i \\ 0.105+26.699i & 10.258+71.229i & 0.153+26.657i & -0.032+16.019i & -0.034+11.322i \\ -0.052+16.037i & 0.153+26.657i & 10.272+71.217i & 0.153+26.657i & -0.052+16.037i \\ -0.034+11.322i & -0.032+16.019i & 0.153+26.657i & 10.258+71.229i & 0.105+26.699i \\ -0.019+8.706i & -0.034+11.322i & -0.052+16.037i & 0.105+26.699i & 10.128+71.349i \end{bmatrix}$$

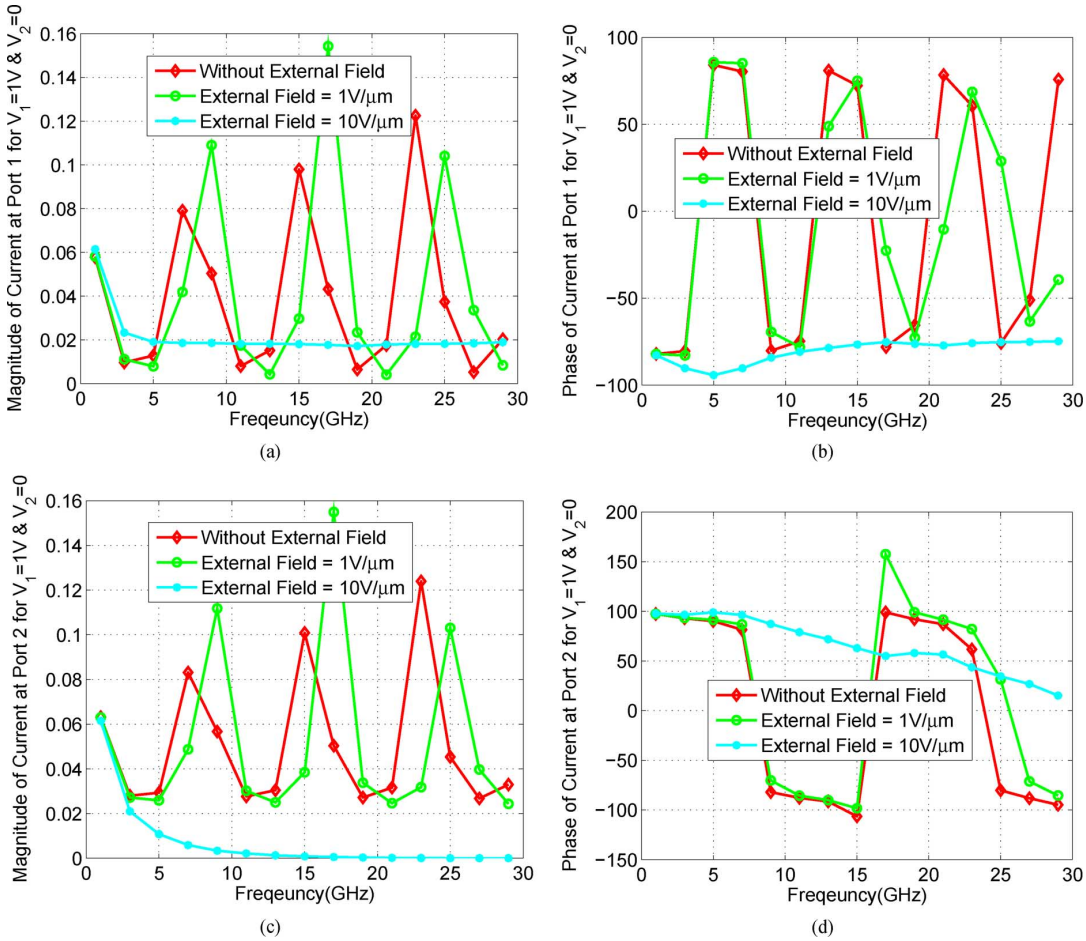

Fig. 7. Currents of a 3-D package interconnect in nonuniform materials with and without external electromagnetic fields. (a) $|I_1|$ (A). (b) Phase (I_1) (degrees). (c) $|I_2|$ (A). (d) Phase (I_2) (degrees).

length of the structure is 1 cm. The conductivity of the metal is 5.8×10^7 S/m.

In Fig. 6, we plot the S-parameters extracted from the proposed VIE solver in comparison with the reference data provided by the Intel Corporation. Once again, excellent agreement is observed in the entire frequency band for all $\mathbf{S}$-parameters.

E. Simulation of Multiple-Dielectric Package Interconnect Exposed to External Fields

Next, we study the circuit performance in the presence of an external electromagnetic field. The package interconnect simulated in Section IV-D is illuminated by an incident plane wave $\vec{E^i}(\vec{r}) = E_0 e^{jk_0 x}\hat{y}$, as shown in Fig. 5, and meanwhile the circuit is attached to circuit sources. In Fig. 7, we plot the currents at each port obtained *without an incident field*, *with an incident field*, and *with a strong incident field*, when port 1 is attached to 1 V, while port 2 is grounded. Port 1 is located at the near end of the conductor in the middle layer, while port 2 is at the far end. It is evident that when a circuit is exposed to a strong external field, its performance can be significantly altered and the circuit can even fail. The currents obtained at each port with one port attached to 1 V and other ports grounded are defined as the $\mathbf{Y}$-parameters of a circuit. When there are external electromagnetic fields, from Fig. 7, it can be seen that the circuit $\mathbf{Y}$-parameters can be significantly changed not only in values, but also in frequency dependence. E_0 is chosen to be comparable to the electric field induced by the circuit source, which is 1 V/μm for the "with an incident field" case, and 10 V/μm for the "with a strong incident field" case, respectively. Since, in this example, the polarization direction of the $\vec{E^i}$ aligns well with the E-field generated by the circuit source, there is a significant impact of the external field on the circuit response when the external field is strong. The current received at port 2 due to the circuit excitation at port 1 can become almost zero at relatively high frequencies since the current induced by the external electromagnetic fields counteracts that generated by the circuit source.

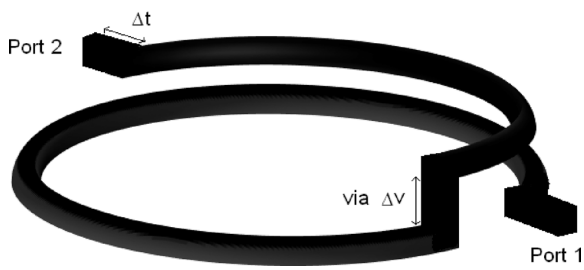

Fig. 8. 3-D view of an irregularly shaped inductor.

F. Simulation of an Irregularly Shaped Spiral Inductor

A two-layer irregularly shaped spiral inductor in free space, as illustrated in Fig. 8, is simulated to demonstrate the flexi-

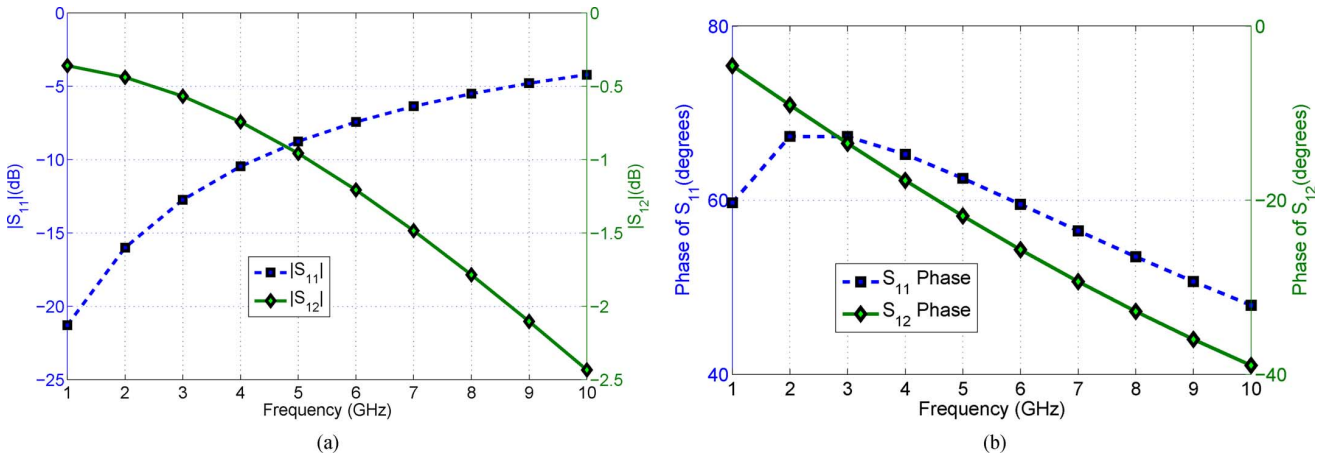

Fig. 9. S-parameters of an irregularly shaped inductor. (a) S_{11} and S_{12} magnitude. (b) S_{11} and S_{12} phase.

bility of the proposed VIE formulation in geometrical modeling. The outer radius of the inductor is 100 μm. The thickness of the metallic wire, the via height Δv, and the port length Δt are all 2 μm. The conductivity of the metal is 5.8×10^7 S/m. Port 1 is located from $\tilde{\phi} = 0$ to $\tilde{\phi} = 10°$ at the lower layer, where $\tilde{\phi}$ denotes the aziumthal angle. Port 2 is located from $\tilde{\phi} = 340°$ to $\tilde{\phi} = 350°$ in the upper layer. The structure is discretized into 348 tetrahedrons. The S-parameters of the inductor from 1 to 10 GHz are simulated by the proposed full-wave VIE formulation. The results are shown in Fig. 9.

V. Conclusions

A new first-principles-based VIE formulation has been developed for the broadband full-wave extraction of general 3-D circuits, containing arbitrarily shaped lossy conductors with inhomogeneous dielectrics. In addition to performing broadband circuit parameter extraction, the proposed VIE formulation also permits the analysis of circuits in the presence of both internal circuit sources and external electromagnetic fields. For such a simultaneous scattering-circuit analysis, as analyzed in this work, the equations that the equivalent currents and charges have to satisfy when the circuit is attached to a circuit source are different from those equations they have to satisfy when the circuit is exposed to an external electromagnetic field. Therefore, one cannot keep the system matrix the same while using both excitations (circuit sources and external electromagnetic fields) in the right-hand side.

The proposed formulation accentuates all the inherent advantages of the VIE formulation traditionally developed for solving wave-related problems, while facilitating circuit parameter extraction such as impedance and scattering parameters at ports located anywhere in the physical structure of a circuit. Besides the VIEs, the method proposed in this paper for incorporating an electric potential-based excitation can also be applied to the surface IEs. In addition to the general setting where ports can be arbitrarily located and be far from each other, the proposed potential-based source model is equally applicable to the setting where the delta-gap source model is valid for use. In the latter case, the proposed potential-based source model helps remove the inaccuracy of the delta-gap source model due to the finite gap width and the artificially introduced conductor for filling the gap. Last, but not least, because of its conformity with the wave-based VIE formulation, the proposed formulation also facilitates the acceleration of its direct solution based on [20] for large-scale computation, which will be explored in the future.

Acknowledgment

The authors would like to thank Dr. J. Morsey, IBM, and Dr. S. Chakravarty, Intel Corporation, for providing interconnect structures and reference data for validation.

References

[1] Z. Zhu, B. Song, and J. K. White, "Algorithms in FastImp: A fast and wideband impedance extraction program for complicated 3-D geometries," *IEEE Trans. Comput.-Aided Design Integr. Circuits Syst.*, vol. 24, no. 7, pp. 981–998, Jul. 2005.

[2] B. Song, Z. Zhu, J. Rockway, and J. White, "A new surface integral formulation for wideband impedance extraction of 3-D structures," in *Int. Comput.-Aided Design Conf.*, San Jose, CA, USA, 2003, pp. 843–847.

[3] Y. Wang, D. Gope, V. Jandhyala, and C. J. R. Shi, "Generalized Kirchhoff's current and voltage law formulation for coupled circuit-electromagnetic simulation with surface integral equations," *IEEE Trans. Microw. Theory Techn.*, vol. 52, no. 7, pp. 1673–1682, Jul. 2004.

[4] W. Chai and D. Jiao, "Direct matrix solution of linear complexity for surface integral-equation based impedance extraction of high bandwidth interconnects," in *48th ACM/EDAC/IEEE Design Automat. Conf.*, San Diego, CA, USA, 2011, pp. 206–211.

[5] W. Chai and D. Jiao, "Direct matrix solution of linear complexity for surface integral-equation based impedance extraction of complicated 3-D structures," *Proc. IEEE (Special Issue)*, vol. 101, no. 2, pp. 372–388, Feb. 2013.

[6] A. E. Ruehli, "Equivalent circuit models for three-dimensional multiconductor systems," *IEEE Trans. Microw. Theory Techn.*, vol. MTT-22, no. 3, pp. 216–221, Mar. 1974.

[7] A. Rong and A. C. Cangellaris, "Generalized PEEC models for three dimensional interconnect structures and integrated passives of arbitrary shapes," in *Proc. Elect. Perform. Electron. Packag. Conf.*, Boston, MA, USA, 2001, pp. 225–228.

[8] A. E. Ruehli, G. Antonini, J. Esch, J. Ekman, A. Mayo, and A. Orlandi, "Nonorthogonal PEEC formulation for time-and frequency-domain EM and circuit modeling," *IEEE Trans. Electromagn. Compat.*, vol. 45, no. 5, pp. 167–176, May 2003.

[9] P. J. Restle, A. E. Ruehli, S. G. Walker, and G. Papadopoulos, "Full-wave PEEC time-domain method for the modeling of on-chip interconnects," *IEEE Trans. Comput.-Aided Design Integr. Circuits Syst.*, vol. 20, no. 7, pp. 877–887, Jul. 2001.

[10] M. Kamon, M. J. Tsuk, and J. K. White, "FastHenry," MIT, Cambridge, MA, USA. [Online]. Available: http://www.rle.mit.edu/cpg/research_codes.htm

[11] M. Kamon, M. J. Tsuk, and J. K. White, "FASTHENRY: A multipole-accelerated 3-D inductance extraction program," *IEEE Trans. Microw. Theory Techn.*, vol. 42, no. 9, pp. 1750–1758, Sep. 1994.

[12] Y. Yi, P. Li, V. Sarin, and W. Shi, "A preconditioned hierarchical algorithm for impedance extraction of three-dimensional structures with multiple dielectrics," *IEEE Trans. Comput.-Aided Design Integr. Circuits Syst.*, vol. 27, no. 11, pp. 1918–1927, Nov. 2008.
[13] D. H. Schaubert, D. R. Wilton, and A. W. Glisson, "A tetrahedral modeling method for electromagnetic scattering by arbitrarily shaped inhomogeneous dielectric bodies," *IEEE Trans. Antennas Propag.*, vol. 32, no. 1, pp. 77–85, Jan. 1984.
[14] M. M. Botha, "Solving the volume integral equations of electromagnetic scattering," *J. Comput. Phys.*, vol. 218, no. 1, pp. 141–158, 2006.
[15] L. E. Sun and W. C. Chew, "A novel formulation of the volume integral equation for general large electromagnetic scattering problems," in *IEEE Int. Antennas Propag. Symp.*, San Diego, CA, USA, 2008, 4 pp.
[16] C.-C. Lu, P. Yla-Oijala, M. Taskinen, and J. Sarvas, "Comparison of two volume integral equation formulations for solving electromagnetic scattering by inhomogeneous dielectric objects," in *IEEE Int. Antennas Propag. Symp.*, Charleston, SC, USA, 2009, 4 pp.
[17] C. Pelletti, G. Bianconi, R. Mittra, and A. Monorchio, "Volume integral equation analysis of thin dielectric sheet using sinusoidal macro-basis functions," *IEEE Antennas Wireless Propag. Lett.*, vol. 12, pp. 441–444, Jul. 2009.
[18] M. I. Sancer, K. Sertel, J. L. Volakis, and P. Van Alstine, "On volume integral equations," *IEEE Trans. Antennas Propag.*, vol. 54, no. 5, pp. 1488–1495, May 2006.
[19] S. Omar and D. Jiao, "A new volume integral equation formulation for analyzing 3-D circuits in inhomogeneous dielectrics exposed to external fields," in *IEEE MTT-S Int. Microw. Symp. Dig.*, Seattle, WA, USA, 2013, 3 pp.
[20] S. Omar and D. Jiao, "An $\mathcal{H}^2$-matrix based fast direct volume integral equation solver for electrodynamic analysis," in *Int. Annu. Rev. Progr. Appl. Comput. Electromagn.*, Columbus, OH, USA, 2012, 6 pp.
[21] R. F. Harrington, *Field Computation by Moment Methods*. Piscataway, NJ, USA: IEEE Press, 1993.
[22] G. P. Junker, A. A. Kishk, and A. W. Glisson, "A novel delta gap source model for center fed cylindrical dipoles," *IEEE Trans. Antennas Propag.*, vol. 43, no. 5, pp. 537–540, May 1995.
[23] Y. H. Lo, S. He, L. Jiang, and W. C. Chew, "Finite-width gap excitation and impedance models," in *IEEE Int. Antennas Propag. Symp.*, Spokane, WA, USA, 2011, pp. 1297–1230.

Saad Omar (S'13) received the B.S.E.E degree (with highest distinction) from the University of Engineering and Technology, Lahore, Pakistan, in 2009, the Masters degree in electrical and computer engineering from Purdue University, West Lafayette, IN, USA, in 2011, and is currently working toward the Ph.D. degree in electrical and computer engineering at Purdue University.

Since 2009, he has been a Research Assistant with the On-Chip Electromagnetics Laboratory, Purdue University, West Lafayette, IN, USA. His current research interests include computational and applied electromagnetics, direct integral equation solvers, inverse scattering problems, fast and high-capacity numerical methods, high-performance very large scale integration (VLSI) computer-aided design (CAD) tools, high-frequency VLSI circuit design and analysis, microwave and millimeter-wave circuits, and bio-electromagnetics.

Dr. Omar is an active member of the IEEE Microwave Theory and Techniques Society (IEEE MTT-S), IEEE Antennas and Propagation Society (AP-S), and Golden Key International Honour Society. He was the recipient of Pakistan's most prestigious Presidential Award, 15 Gold Medals, and the National Talent Scholarship for his record-breaking academic performances both in pre-engineering and engineering schools.

Dan Jiao (S'00–M'02–SM'06) received the Ph.D. degree in electrical engineering from the University of Illinois at Urbana-Champaign, Urbana, IL, USA, in 2001.

From 2001 to 2005, she was with the Technology Computer-Aided Design (CAD) Division, Intel Corporation, as a Senior CAD Engineer, Staff Engineer, and Senior Staff Engineer. In September 2005, she joined Purdue University, West Lafayette, IN, as an Assistant Professor with the School of Electrical and Computer Engineering, where she is currently a Professor. She has authored two book chapters and over 180 papers in refereed journals and international conferences. Her current research interests include computational electromagnetics, high-frequency digital, analog, mixed-signal, and RF integrated circuit (IC) design and analysis, high-performance very large-scale integration (VLSI) computer-aided design (CAD), modeling of microscale and nanoscale circuits, applied electromagnetics, fast and high-capacity numerical methods, fast time-domain analysis, scattering and antenna analysis, RF, microwave, and millimeter-wave circuits, wireless communication, and bio-electromagnetics.

Dr. Jiao has been a reviewer for many IEEE journals and conferences. She is an associate editor for the IEEE TRANSATCTIONS ON COMPONENTS, PACKAGING, AND MANUFACTURING TECHNOLOGY. She was the recipient of the 2013 S. A. Schelkunoff Prize Paper Award of the IEEE Antennas and Propagation Society, which recognizes the Best Paper published in the IEEE TRANSACTIONS ON ANTENNAS AND PROPAGATION from the previous year. Since 2013, she has been a University Faculty Scholar of Purdue University. She was among the 85 engineers selected throughout the nation for the National Academy of Engineering's 2011 U.S. Frontiers of Engineering Symposium. She was the recipient of the 2010 Ruth and Joel Spira Outstanding Teaching Award, the 2008 National Science Foundation (NSF) CAREER Award, the 2006 Jack and Cathie Kozik Faculty Start Up Award (which recognizes an outstanding new faculty member of the School of Electrical and Computer Engineering, Purdue University), a 2006 Office of Naval Research (ONR) Award under the Young Investigator Program, the 2004 Best Paper Award presented at Intel Corporation's annual corporate-wide technology conference (Design and Test Technology Conference) for her work on a generic broadband model of high-speed circuits, the 2003 Intel Corporation Logic Technology Development (LTD) Divisional Achievement Award, the Intel Corporation Technology CAD Divisional Achievement Award, the 2002 Intel Corporation Components Research the Intel Hero Award (Intel-wide she was the tenth recipient), the Intel Corporation LTD Team Quality Award, and the 2000 Raj Mittra Outstanding Research Award presented by the University of Illinois at Urbana-Champaign.